Cellular dynamics emerging from turbulent flows steered by active filaments

Mehrana R. Nejad [1,2,*] Julia M. Yeomans [3] and Sumesh P. Thampi [3,4]

[1]*Department of Physics, Harvard University, Cambridge, Massachusetts 02138, USA*

[2]*School of Engineering and Applied Sciences, Harvard University, Cambridge, Massachusetts 02138, USA*

[3]*The Rudolf Peierls Centre for Theoretical Physics, Department of Physics, University of Oxford, Parks Road, Oxford OX1 3PU, United Kingdom*

[4]*Department of Chemical Engineering, Indian Institute of Technology, Madras, Chennai 600 036, India*

(Received 31 March 2025; accepted 23 September 2025; published 17 October 2025)

We develop a continuum theory to describe the collective dynamics of deformable epithelial cells, distinguishing the force-generating active filaments in the cells from their shape. The theory demonstrates how active flows driven by active filaments can create nematic domains and topological defects in the cell shape field. We highlight the role of the filament flow-aligning parameter, λ_Q, a rheological quantity that determines the response of the filaments to velocity gradients in the active flows, and plays a significant, to date unappreciated, role in determining the pattern of extensional and compressional active flows. In a contractile cell layer, local flows are expected to align elongated cells perpendicular to the active filaments. However, with increasing λ_Q, long-range correlations in the active turbulent flow field lead to extended regions where this alignment is parallel, consistent with recent experiments on confluent Madin-Darby canine kidney (MDCK) cell layers. Further, we distinguish defects in the filament director field, which contribute to the active driving, and those in the shape director field, measured in experiments, which are advected by the active flows. By considering the shape-filament orientation, we explain the unexpected motion of $+1/2$ defects towards their head in contractile cell layers, consistent with recent experiments on epithelial layers examining stress around shape defects.

DOI: 10.1103/mmyk-f9x3

I. INTRODUCTION

Active matter describes materials that operate out of thermodynamic equilibrium, harnessing energy from their surroundings to do work. A canonical example is living matter which transforms chemical energy to growth and movement, the hallmarks of life. This has sparked significant interest in the biophysics community in applying active matter physics to investigate mechanical and developmental processes in biology [1–5]. Examples include correlated tissue flows in embryogenesis [6,7], wound healing [8,9], and cancer development and metastasis [10,11].

Epithelia are an important class of tissues that include the skin and the lining of hollow organs such as the lungs. Epithelial cells often form tightly connected, two-dimensional layers, and well-studied in vitro model systems consist of confluent layers of epithelial cells cultured on a substrate [8,12–16]. The activity of the cells can result in complex, dynamical behavior, including flocking [3,17] and active turbulence [18,19]. Recent studies have increasingly highlighted the significance of epithelial dynamics in organoids and *in vivo* [20–22].

The biological processes involved in collective cell motion are complex and poorly understood, and experimental observations are diverse. A powerful approach to address these challenges is to develop coarse-grained, physical theories which bypass cellular details, but remain grounded in conservation laws and symmetries. A successful example is the continuum theory of active nematics, which has offered a framework to explain many properties of dense suspensions of nondeformable, active particles such as that of bacteria and cytoskeletal filaments. These include the dynamical state of active turbulence, characterized by jets and vortices of the velocity field, and the dynamics of topological defects [23–25]. These theories have also been helpful to understand the dynamics of deformable particles such as cell monolayers driven by nonequilibrium forces from stress-generating active filaments [26–29], cellular division [30,31], or topological rearrangements [32,33], the presence of topological defects triggering cell extrusion [18,34], and motility and spontaneous oscillations arising from self-generated flows [14,16,35–37].

However, almost all these studies assume that the microstructure of cell collectives can be described by a single tensor order parameter, the $\boldsymbol{Q}$ tensor, which represents the nematic order in the system [18,38]. The literature variously interprets the $\boldsymbol{Q}$ tensor as referring to force generating active filaments or cellular shape [18,27,34–36]. Here, we demonstrate the necessity of distinguishing between the shape of the cells and the internal stress generating active filaments, showing that two tensor order parameters are required to capture many features of the collective dynamical behavior of cells. Previous works on continuum models that accounted for cell shapes focused on the rheological consequences of cellular deformations [39–41], primarily through passive mechanisms. In contrast, we illustrate how filamental network and cellular

*Contact author: mehrana@g.harvard.edu

shapes can be coupled through the active filament driven fluid flows and thus generate nematic order and topological defects in cell shape.

In the next section we introduce the model. An active nematic field, representing active filaments, produces flows while a second tensor field describes cell shape which can be influenced by the active flows. Our coupled equations of motion predict the emergence of locally extensional flows within a contractile active material—an outcome consistent with recent experimental findings [42]. Furthermore by differentiating topological defects in the filament and shape fields we show that $+\frac{1}{2}$ shape defects can move towards their heads in a contractile system. Our analysis, thus, makes connections with very recent experimental observations of misalignment between stress fibers and cell shapes associated with $+\frac{1}{2}$ topological defects [43].

II. THEORY

We use a continuum approach and describe the dynamics of a two-dimensional layer of confluent cells using a vector velocity field $\boldsymbol{u}$ and two tensor order parameter fields for the microstructure, $\boldsymbol{Q}$ and $\boldsymbol{W}$. The rank-2 tensor $\boldsymbol{Q}$, referred to as the filament order parameter, represents the nematic orientational order of the filaments that form the cytoskeletal network. As is well studied in the active nematic literature, $\boldsymbol{Q}$ is a traceless, symmetric tensor; the eigenvalues and eigenvectors give the magnitude of the orientational order, S, and the director field respectively [44–46]. Motor proteins bound to the cytoskeletal filaments generate internal stresses in the cellular layer using the energy derived from adenosine triphosphate (ATP) hydrolysis, as demonstrated through both *in vivo* and *in vitro* experiments [16,18,47]. We model these by including a term that generates active stresses and flows in the equations of motion [46,48,49].

Active flows, cell-cell adhesion, cellular processes, and mechanical stress are known to affect the cell shape [9,50], which may evolve independently from the dynamics of the cytoskeletal filamentous network [42,51]. To account for this, we introduce a second structural variable to describe cell shape, a quantity often characterized in experiments. The shape order parameter $\boldsymbol{W}$ is a traceless, symmetric, rank-2 tensor that quantifies anisotropy in the cell shape. $\boldsymbol{W} = \boldsymbol{0}$ corresponds to isotropic cells, and the eigenvalues and eigenvectors of $\boldsymbol{W}$ give the magnitude of the anisotropy of the cells and the direction of the corresponding deformation, respectively, as discussed in [52].

The velocity field obeys the continuity and Navier-Stokes equations,

$$\boldsymbol{\nabla} \cdot \boldsymbol{u} = 0, \tag{1}$$

$$\rho(\partial_t + \boldsymbol{u} \cdot \boldsymbol{\nabla})\boldsymbol{u} = \boldsymbol{\nabla} \cdot \boldsymbol{\Pi}. \tag{2}$$

Here, ρ is the local density and $\boldsymbol{\Pi}$ is a generalized stress tensor that contains contributions from active cellular processes and (passive) viscoelastic effects.

The two tensor order parameters are advected by the flow fields, and evolve in response to flow gradients and thermodynamic driving forces. Thus,

$$\partial_t \boldsymbol{Q} = -\boldsymbol{u} \cdot \boldsymbol{\nabla}\boldsymbol{Q} + \mathbf{S}_{\boldsymbol{Q}} + \Gamma_{\boldsymbol{Q}} \boldsymbol{H}_{\boldsymbol{Q}}, \tag{3}$$

$$\partial_t \boldsymbol{W} = -\boldsymbol{u} \cdot \boldsymbol{\nabla}\boldsymbol{W} + \mathbf{S}_{\boldsymbol{W}} + \Gamma_{\boldsymbol{W}} \boldsymbol{H}_{\boldsymbol{W}}, \tag{4}$$

where, for $\boldsymbol{R} \in \{\boldsymbol{Q}, \boldsymbol{W}\}$, $\partial_t \boldsymbol{R} + \boldsymbol{u} \cdot \boldsymbol{\nabla}\boldsymbol{R} - \mathbf{S}_{\boldsymbol{R}}$ is the convected derivative for the tensor order parameter field $\boldsymbol{R}$ and

$$\mathbf{S}_{\boldsymbol{R}} = (\lambda_{\boldsymbol{R}} \boldsymbol{E} + \boldsymbol{\Omega}) \cdot \left(\boldsymbol{R} + \frac{\boldsymbol{I}}{2}\right) + \left(\boldsymbol{R} + \frac{\boldsymbol{I}}{2}\right) \cdot (\lambda_{\boldsymbol{R}} \boldsymbol{E} - \boldsymbol{\Omega}) - \lambda_{\boldsymbol{R}} \left(\boldsymbol{R} + \frac{\boldsymbol{I}}{2}\right)(\boldsymbol{R} : \boldsymbol{\nabla}\boldsymbol{u}). \tag{5}$$

The strain rate tensor and the vorticity tensor are defined as $\boldsymbol{E} = (\boldsymbol{\nabla}\boldsymbol{u}^T + \boldsymbol{\nabla}\boldsymbol{u})/2$ and $\boldsymbol{\Omega} = (\boldsymbol{\nabla}\boldsymbol{u}^T - \boldsymbol{\nabla}\boldsymbol{u})/2$, respectively, representing the symmetric and antisymmetric parts of the velocity gradient tensor.

Different weights are given to the symmetric and antisymmetric parts of the velocity gradient tensor in coupling with the field $\boldsymbol{R}$ through the parameter $\lambda_{\boldsymbol{R}}$. The filament flow-aligning parameter $\lambda_{\boldsymbol{Q}}$, also known as flow-tumbling parameter in the liquid crystal literature, is a rheological quantity that is related to the Leslie coefficients of anisotropic viscosity [45]. For nematogens with fixed shape, this parameter is a function of aspect ratio and orientational order, and it determines the aligning/tumbling behavior of active filaments in a simple shear flow. Analogously, we have $\lambda_{\boldsymbol{W}}$ as a shape flow-aligning parameter. For deformable particles, this coefficient is positive and leads to the elongation of the particles along the principal directions of the velocity gradient tensor. In the limit $\lambda_{\boldsymbol{W}} \to 0$ flow gradients merely rotate the tensor field $\boldsymbol{W}$; that is, cells do not undergo any deformation but they undergo rigid body rotation in accordance with the local vorticity tensor. We take $\lambda_{\boldsymbol{W}} > 0$ in this study. Although we consider an effective velocity field that governs the dynamics of both the cells and the filaments, their different flow-aligning parameters lead to distinct responses in shear flows.

Further, $\Gamma_{\boldsymbol{R}}$ is the orientational relaxation time and

$$\boldsymbol{H}_{\boldsymbol{R}} = -\frac{\delta \mathcal{F}_{\boldsymbol{R}}}{\delta \boldsymbol{R}} + \frac{\boldsymbol{I}}{2}\mathrm{Tr}\left(\frac{\delta \mathcal{F}_{\boldsymbol{R}}}{\delta \boldsymbol{R}}\right) \tag{6}$$

is the molecular potential derived from the variational derivative of the free energy $\mathcal{F}_{\boldsymbol{R}} = \int f_{\boldsymbol{R}} d\mathcal{V}$, where $\boldsymbol{I}$ is the identity tensor and $\mathrm{Tr}(\cdot)$ is the trace of the tensor argument. The free energy density $f_{\boldsymbol{R}}$ is

$$f_{\boldsymbol{R}} = f^b_{\boldsymbol{R}} + \frac{K_{\boldsymbol{R}}}{2}|\boldsymbol{\nabla}\boldsymbol{R}|^2, \tag{7}$$

where the bulk terms are chosen as $f^b_{\boldsymbol{Q}} = \frac{C_{\boldsymbol{Q}}}{4}(1 - 3\boldsymbol{Q} : \boldsymbol{Q})^2$ and $f^b_{\boldsymbol{W}} = \frac{C_{\boldsymbol{W}}}{4}(1 + \boldsymbol{W} : \boldsymbol{W})^2$. $f^b_{\boldsymbol{Q}}$ corresponds to the usual Landau–de Gennes free energy contribution for the $\boldsymbol{Q}$ tensor field [44] while $f^b_{\boldsymbol{W}}$ ensures that the shape tensor corresponds to isotropic cells in the absence of activity. The second term in the free energy determines the contribution arising from the gradients in the field variable (Frank elasticity) assuming a single elastic constant, $K_{\boldsymbol{R}}$. Here, unlike in [42], we have no free energy mediated aligning between the cell shape and the active filaments, in order to isolate the role of activity in the alignment/misalignment between the two.

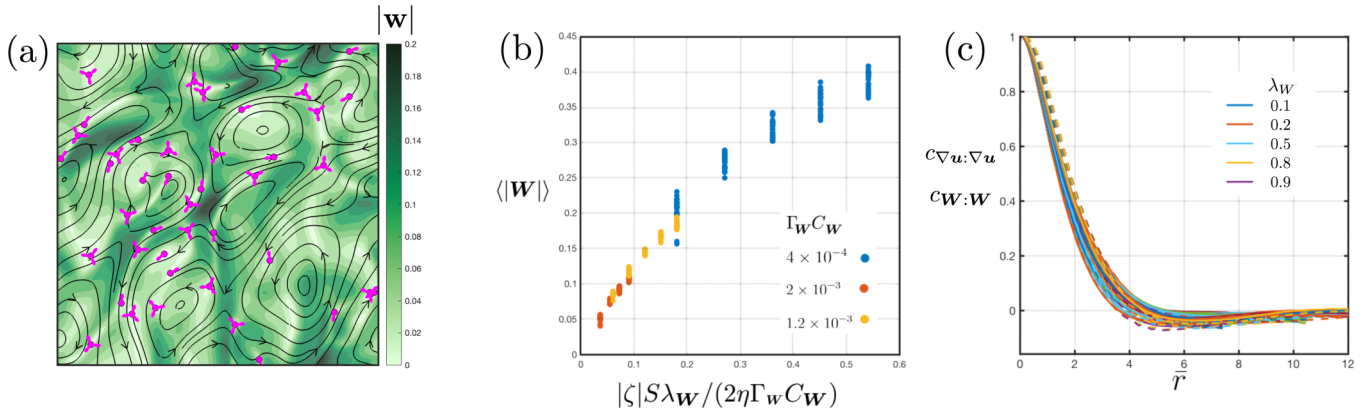

FIG. 1. Active flows form elongated, nematically ordered cells. (a) Active turbulence illustrated using the velocity streamlines. The domain is colored with cell elongation $|\boldsymbol{W}|$. Comet-shaped and trefoil-shaped symbols are $\pm\frac{1}{2}$ topological defects in the nematic order of the cell shape field. (b) $\langle|\boldsymbol{W}|\rangle$, spatiotemporally averaged magnitude of cell elongation, as a function of contractile activity $|\zeta|$ of the filaments. Here, $\lambda_{\boldsymbol{W}} = 1$. Markers of same color, that appear vertically placed, result from different values of ζ and $\lambda_{\boldsymbol{Q}}$. (c) Spatial correlations in the shape tensor $c_{\boldsymbol{W}:\boldsymbol{W}}(r)$ (continuous lines) and the velocity gradient tensor $c_{\nabla\boldsymbol{u}:\nabla\boldsymbol{u}}$ (dashed lines) as a function of distance $\bar{r} = r/l_a$, which is normalized by the active length scale $l_a = \sqrt{K_{\boldsymbol{Q}}/|\zeta|}$, for various values of activity, $\zeta \in \{\pm 0.01, \pm 0.02, \pm 0.03\}$. The correlation functions are defined as $c_{\boldsymbol{X}:\boldsymbol{X}}(r) = (\langle \boldsymbol{X}(\mathbf{r}_0) : \boldsymbol{X}(\mathbf{r}_0 + \mathbf{r})\rangle)/(\langle \boldsymbol{X}(\mathbf{r}_0) : \boldsymbol{X}(\mathbf{r}_0)\rangle)$, where $\boldsymbol{X} \in \{\nabla\boldsymbol{u}, \boldsymbol{W}\}$ and $\langle\rangle$ shows the average over space r_0 and over time.

While the spatiotemporal evolution of the two order parameters $\boldsymbol{Q}$ and $\boldsymbol{W}$ is driven by the flow field $\boldsymbol{u}$, the two microstructural variables also dictate the dynamics of the cellular layer through the stress, $\boldsymbol{\Pi}$, in Eq. (2). The stress field includes both active and passive contributions. The active contribution, $\boldsymbol{\Pi}^{\mathrm{a}} = -\zeta\mathbf{Q}$, arises from the internal stress generated by the action of molecular motors on the cytoskeletal filaments. The activity coefficient ζ that determines the strength of active stress is positive for extensile nematogens that pump fluid outwards away from their ends and negative for contractile particles that draw fluid inwards towards their ends.

The passive part includes the isotropic contribution $\boldsymbol{\Pi}^{\mathrm{i}} = -P\boldsymbol{I}$, where P is the pressure, the viscous stress, $\boldsymbol{\Pi}^{\mathrm{v}} = 2\eta\boldsymbol{E}$, where η is the medium viscosity, and elastic stresses arising from the two tensor order parameters,

$$\boldsymbol{\Pi}^{\mathrm{e}}{}_{\boldsymbol{R}} = 2\lambda_{\boldsymbol{R}}\boldsymbol{R}(\boldsymbol{R} : \boldsymbol{H}_{\boldsymbol{R}}) - \lambda_{\boldsymbol{R}}(\boldsymbol{H}_{\boldsymbol{R}} \cdot \boldsymbol{R} + \boldsymbol{R} \cdot \boldsymbol{H}_{\boldsymbol{R}}) - \nabla\boldsymbol{R} : \frac{\delta\mathcal{F}_{\boldsymbol{R}}}{\delta\nabla\boldsymbol{R}} + \boldsymbol{R} \cdot \boldsymbol{H}_{\boldsymbol{R}} - \boldsymbol{H}_{\boldsymbol{R}} \cdot \boldsymbol{R}. \tag{8}$$

III. SIMULATIONS

We use a hybrid lattice Boltzmann method [53,54] to solve the set of governing equations (1)–(4). The simulations were initialized with a quiescent fluid ($\boldsymbol{u} = 0$), with randomly oriented active filaments ($\boldsymbol{Q}$) and shapes ($\boldsymbol{W}$) in a domain of 150×150 with periodic boundary conditions. Data were collected after the simulations reached a statistically steady state. Unless otherwise stated the parameters used in the simulations were $C_{\boldsymbol{Q}} = C_{\boldsymbol{W}} = 10^{-3}$, $K_{\boldsymbol{Q}} = 10^{-2}$, $K_{\boldsymbol{W}} = 0$, $\Gamma_{\boldsymbol{Q}} = \Gamma_{\boldsymbol{W}} = 0.4$, $\rho = 40$, $\eta = 40/3$, and $\zeta = \pm 0.01$. Inertial effects are negligible, and the typical Reynolds number in the simulations is $\sim 10^{-3}$.

The active stress $\boldsymbol{\Pi}^{a}$ that arises from the activity of molecular motors on the filaments results in the well-known hydrodynamic instabilities of active nematics. This results in an active turbulent state that is sustained through the formation and destruction of domain walls and topological defects in the nematically ordered filaments [55–57]. The simulation parameters are chosen to ensure that the state of active turbulence prevails, and that topological defects are formed and annihilated continuously, as observed in experiments on epithelial tissues. Our results on the direction of defect motion and the emergence of alignment between cells and filaments—perpendicular in contractile and parallel in extensile systems—remain valid for other parameter sets that yield an active steady state with defects.

IV. CELLS ARE ELONGATED BY ACTIVE FLOWS

The active turbulent flow field consists of fluid jets and vortices [36,54,58] as shown in Fig. 1(a). The straining flows of active turbulence in a confluent cell layer deform the otherwise isotropic cells. The shading in the figure shows the magnitude of the shape tensor field, $|\boldsymbol{W}|$, indicating the extent of this deformation. Further, Fig. 1(b) plots the anisotropy of the cells, quantified as the average magnitude of the shape tensor, $\langle|\boldsymbol{W}|\rangle$, as a function of the contractile activity of the filaments, $|\zeta|$.

Examining Eq. (4) for a homogeneous steady-state solution for the shape tensor, for small deformations ($|\boldsymbol{W}| \ll 1$) we obtain

$$\boldsymbol{W} \sim \frac{\lambda_{\boldsymbol{W}}}{\Gamma_{\boldsymbol{W}} C_{\boldsymbol{W}}}\boldsymbol{E}, \tag{9}$$

confirming that the straining flows of active turbulence indeed deform the cells with the direction of deformation along the principal axis of the strain rate tensor, $\boldsymbol{E}$. Balancing the viscous and active stress in the momentum balance [Eq. (2)] gives

$$\boldsymbol{E} \sim \frac{\zeta}{2\eta}\boldsymbol{Q}. \tag{10}$$

Eliminating $\boldsymbol{E}$ from Eq. (9) using Eq. (10), we obtain a linear scaling for the deformation of the cells $|\boldsymbol{W}| \sim |\zeta|\lambda_{\boldsymbol{W}} S/(2\eta\Gamma_{\boldsymbol{W}} C_{\boldsymbol{W}})$, consistent with the data reported in

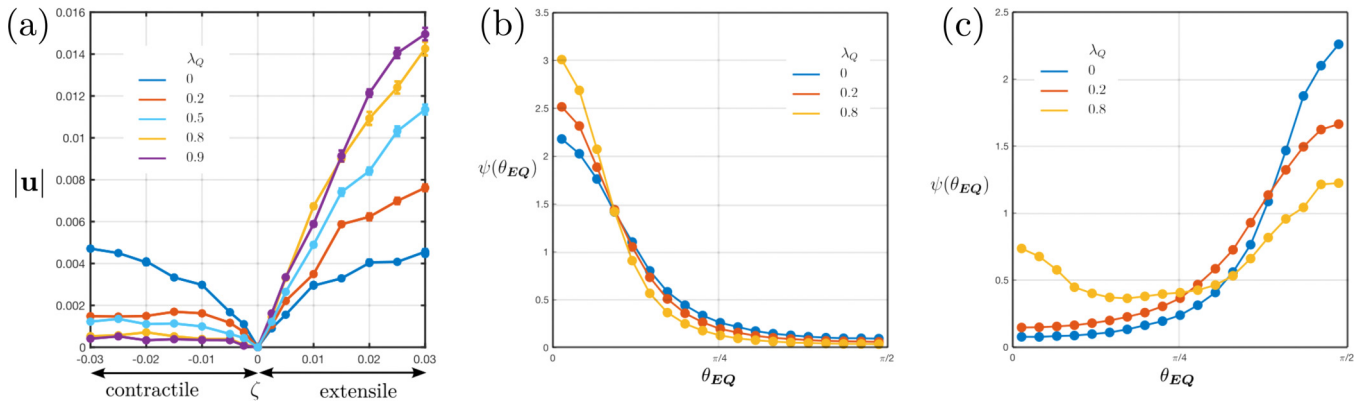

FIG. 2. Dependence of the active turbulent flow field on the filament flow-aligning parameter $\lambda_{\boldsymbol{Q}}$. (a) Average speed of the fluid as a function of filament activity. (b,c) Probability density function $\psi(\theta_{\boldsymbol{EQ}})$ describing the distribution of $\theta_{\boldsymbol{EQ}}$, the angle between the dominant eigenvectors of the rate of strain tensor and the filament order parameter in an active turbulent flow field in (b) extensile and (c) contractile systems. $\psi(\theta_{\boldsymbol{EQ}})$ is normalized so that the area under the graph is equal to 1.

Fig. 1(b). At higher activities, the scaling breaks down since the elongation of cells is not small and the contribution of nonlinear terms in the free energy is not negligible.

In order to probe whether the anisotropic cells develop spatial nematic order, even given our choice of elastic constant $K_{\boldsymbol{W}} = 0$, we measure the spatial correlations of the shape tensor, $\langle \boldsymbol{W}(\mathbf{r}_0) : \boldsymbol{W}(\mathbf{r}_0 + \mathbf{r})\rangle$, normalized by $\langle |\boldsymbol{W}(\mathbf{r}_0)|^2\rangle$ and plotted in Fig. 1(c). The spatial correlations in the velocity gradient tensor, $\langle \nabla \boldsymbol{u}(\mathbf{r}_0) : \nabla \boldsymbol{u}(\mathbf{r}_0 + \mathbf{r})\rangle$, normalized by $\langle |\nabla \boldsymbol{u}(\mathbf{r}_0)|^2\rangle$, which decay over the active length scale $\sim\sqrt{K_{\boldsymbol{Q}}/|\zeta|}$, are also shown for comparison. The spatial nematic order of anisotropic cells persists on the active length scale, and behaves similarly to the spatial correlations in the velocity gradient field, as expected since the former is driven by the latter. Similarly, both shape deformations and flows persist over the active time scale, $\tau_a \sim \eta/\zeta$ [59] (see Fig. 5 in Appendix A). Hence, activity alone can lead to both elongation and spatial nematic order of the elongated cells without the need for any thermodynamic driving forces.

While straining flows generated by activity elongate the deformable cells, the corresponding vortical field (antisymmetric part of the velocity gradient tensor) simultaneously rotates them. Therefore, the filament flow-aligning parameter $\lambda_{\boldsymbol{Q}}$ and the shape flow-aligning parameter $\lambda_{\boldsymbol{W}}$—that respectively control the response of the nematic order parameter of the filaments $\boldsymbol{Q}$ and that of the shape order parameter of the cells $\boldsymbol{W}$ to the strain rate and vorticity tensors—play an important role in determining the deformation of the cells. Irrespective of the value of $\lambda_{\boldsymbol{Q}}$, an increase in $\lambda_{\boldsymbol{W}}$ leads to greater elongation of the cells in accordance with Eq. (9). The role of the filament flow-aligning parameter $\lambda_{\boldsymbol{Q}}$ depends on the details of the active turbulent flow field, which we now discuss in more detail.

V. PROPERTIES OF THE ACTIVE TURBULENT FLOW FIELD

Figure 2(a) plots the mean speed of the active turbulent flows for various values of the filament flow-aligning parameter, comparing the contractile and the extensile cases. For $\lambda_{\boldsymbol{Q}} = 0$, the velocities are similar in extensile and contractile systems, but they increase with $\lambda_{\boldsymbol{Q}}$ in an extensile system and decrease with $\lambda_{\boldsymbol{Q}}$ in a contractile system. To explain this we consider the different characteristics of extensile and contractile active flows. Equation (3) suggests that, to the leading order,

$$\partial_t \boldsymbol{Q} \sim \lambda_{\boldsymbol{Q}} \boldsymbol{E}, \tag{11}$$

and, combining Eqs. (10) and (11), we have $\partial_t \boldsymbol{Q} \sim \frac{\zeta \lambda_{\boldsymbol{Q}}}{2\eta} \boldsymbol{Q}$. Thus, in an extensile system for which $\zeta > 0$, there is a bootstrapping effect: active flows enhance nematic order, leading to stronger flows emerging from active hydrodynamic instabilities. On the other hand, contractile systems, for which $\zeta < 0$, oppose the buildup of nematic order, resulting in weaker active turbulent flows. While the nature of the active flow induced nematic ordering (or disruption) is dictated by whether the system is extensile or contractile (sign of ζ), the strength of the effect is also influenced by the filament flow-aligning parameter $\lambda_{\boldsymbol{Q}}$. Thus, an increase in $\lambda_{\boldsymbol{Q}}$ increases the mean speed in extensile systems and decreases it in the contractile case.

Furthermore, the filament flow-aligning parameter affects the nature of the straining flows in active turbulence. An active turbulent velocity field consists of regions of extensional and compressional flows, which are distinguished locally based on the alignment of the strain rate tensor with respect to the orientation of the active filaments. To help to clarify the relation between the straining flow and the filament orientation we will call the flows extensional when the extensional axis of the flow (the eigenvector of the strain rate tensor corresponding to the largest positive eigenvalue) is parallel to the axis of the active filaments, i.e., $\boldsymbol{E} \parallel \boldsymbol{Q}$. Similarly, we will call the flows compressional when the extensional axis of the flow is perpendicular to the axis of the filaments, i.e., $\boldsymbol{E} \perp \boldsymbol{Q}$. Local extensional flows are characteristic of extensile filaments and local compressional flows are characteristic of contractile filaments.

Figures 2(b) and 2(c) plot $\psi(\theta_{\boldsymbol{EQ}})$, the probability density function of the angle between the dominant eigenvector of the strain rate tensor and the director field of the active filaments in extensile and contractile systems respectively. When $\lambda_{\boldsymbol{Q}} = 0$, the distribution $\psi(\theta_{\boldsymbol{EQ}})$ peaks at $\theta_{\boldsymbol{EQ}} = 0$ for

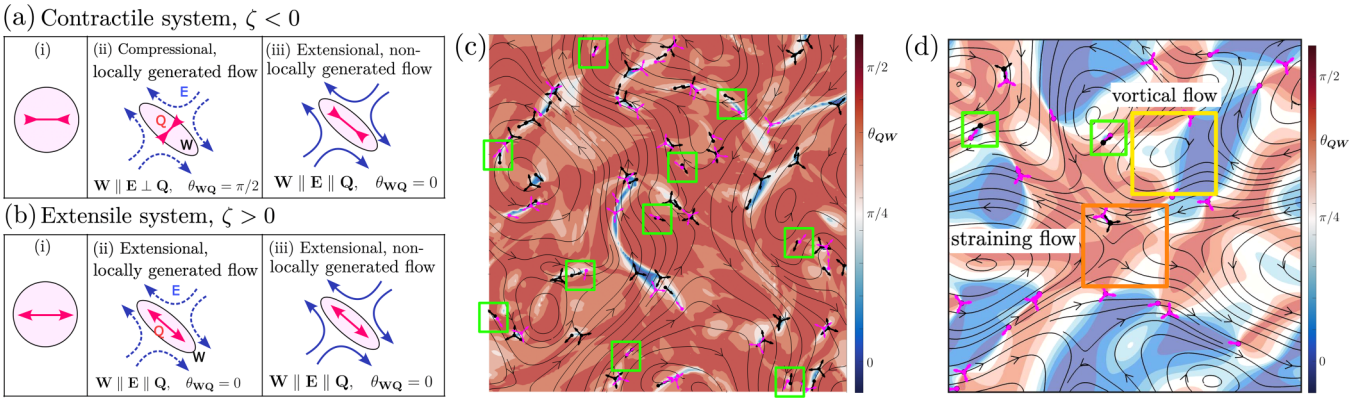

FIG. 3. Elongated cells and active filaments orient in distinct ways in active turbulence. (a) Contractile system: (i) isotropic cells (shaded circles) with contractile filaments (double-headed arrows) deformed by (ii) local compressional flows (dashed, blue arrows) and (iii) nonlocal extensional flows (solid, blue arrows) of active turbulence. (b) Extensile system: (i) isotropic cells (shaded circles) with extensile filaments (double-headed arrows) deformed by (ii) local extensional flows (dashed, blue arrows) and (iii) nonlocal extensional flows (solid, blue arrows) of active turbulence. (c), (d) Snapshots of the active turbulent domains in a contractile system ($\zeta < 0$) colored with the alignment angle $\theta_{\boldsymbol{WQ}}$, the angle between the director of elongated cells and active filaments for (c) $\lambda_{\boldsymbol{Q}} = 0$ and (d) $\lambda_{\boldsymbol{Q}} = 0.8$. The continuous lines are velocity streamlines. The half-integer defects in the nematic order of filaments and elongated cells are colored in black and magenta, respectively. Green outlines show examples of antiparallel configuration of $+1/2$ defects in shape and filaments that are close to each other. The orange and yellow boxes in (d) are, respectively, examples of straining and vortical flows.

extensile systems and at $\theta_{\boldsymbol{EQ}} = \pi/2$ for contractile systems, as expected. These distributions are nearly mirror images of each other. However, the distributions and the symmetry in the distributions change with variations in filament flow-aligning parameter $\lambda_{\boldsymbol{Q}}$. With an increase in $\lambda_{\boldsymbol{Q}}$, the distribution $\psi(\theta_{\boldsymbol{EQ}})$ remains unimodal and the peak at $\theta_{\boldsymbol{EQ}} = 0$ becomes sharper for extensile filaments. For contractile filaments, an increase in $\lambda_{\boldsymbol{Q}}$ weakens the peak at $\theta_{\boldsymbol{EQ}} = \pi/2$, and the distribution becomes bimodal with the appearance of a new peak at $\theta_{\boldsymbol{EQ}} = 0$. To summarize, with an increase in the filament flow-aligning parameter, extensional flows get stronger in an extensile system while domains of extensional flows develop in an otherwise compressional contractile system.

The existence of extensional flows in a contractile system conflicts with the approximate, local active-viscous stress balance anticipated from Eq. (10); instead nematic ordering of the filaments develop as a consequence of nonlocal hydrodynamics. A net straining flow is produced in a region due to viscous diffusion of momentum generated elsewhere in the field, a characteristic of Stokesian flows. In such straining flows, active filaments can rotate to align along the extensional axis, producing regions of extensional flow, $\theta_{\boldsymbol{EQ}} = 0$. Since the mechanism, which again follows from Eq. (11), is dependent on the filament flow-aligning parameter, the strength of the peak at $\theta_{\boldsymbol{EQ}} = 0$ increases with an increase in $\lambda_{\boldsymbol{Q}}$.

On the other hand, nonlocally generated flows do not give rise to such distinct and contrasting flow regions in extensile systems, since filaments already tend to orient along the extensional axis of local flows, and hence the peak at $\theta_{\boldsymbol{EQ}} = 0$ is only enhanced with an increase in $\lambda_{\boldsymbol{Q}}$.

VI. ALIGNMENT BETWEEN ACTIVE FILAMENTS AND ELONGATED CELLS

We have confirmed in previous sections that the cells are predominantly deformed along the principal axis of the strain rate tensor, $\boldsymbol{W} \parallel \boldsymbol{E}$, and shown that, in contractile active turbulence, extensional flows may emerge causing the angle between $\boldsymbol{E}$ and the filament director $\boldsymbol{Q}$ to take a range of values between 0 and $\pi/2$. We now discuss how this affects the angle $\theta_{\boldsymbol{WQ}}$ between the orientation of the active filaments and the cell elongation axis.

Consider a system of isotropic cells (shaded circles) powered by co-occurring active filaments (two-headed arrows) shown schematically in column (i) in Fig. 3(a). If the active filaments are contractile (shown by inward-pointing arrows), $\zeta < 0$ and active-viscous stress balance [Eq. (10)] suggests that $\boldsymbol{E} \perp \boldsymbol{Q}$. That is, the active, straining fluid flows are compressional along the filament director axis, as expected for a contractile force dipole. But cells elongate along the extensional axis of the flow [in accordance with Eq. (9)] resulting in $\boldsymbol{W} \parallel \boldsymbol{E} \perp \boldsymbol{Q}$ [column (ii) in Fig. 3(a)].

However, we have argued that, as $\lambda_{\boldsymbol{Q}}$ increases, active turbulence can also produce effective extensional flows in contractile systems, i.e., regions with $\boldsymbol{E} \parallel \boldsymbol{Q}$. Isotropic cells deform along the extensional axis of the prevailing local flow as before, resulting in $\boldsymbol{W} \parallel \boldsymbol{E} \parallel \boldsymbol{Q}$ [column (iii) in Fig. 3(a)].

We highlight this behavior in snapshots of contractile active turbulence in Figs. 3(c) and 3(d), where the domains are colored based on $\theta_{\boldsymbol{WQ}}$, the angle between the director fields of the shape and of the active filaments. Regions with $\theta_{\boldsymbol{WQ}} \approx \frac{\pi}{2}$ are colored red, and regions with $\theta_{\boldsymbol{WQ}} \approx 0$ are colored blue.

For $\lambda_{\boldsymbol{Q}} = 0$ and contractile filaments Fig. 2(c) indicates that $\boldsymbol{E}$ is typically perpendicular to $\boldsymbol{Q}$. Therefore case (ii) in Fig. 3(a) holds, $\theta_{\boldsymbol{WQ}} \approx \frac{\pi}{2}$, almost everywhere, and the domain in Fig. 3(c) is almost entirely red. For $\lambda_{\boldsymbol{Q}} = 0.8$, however, a large fraction of filaments become elongated in the same direction as the extensional flows, $\boldsymbol{E} \parallel \boldsymbol{Q}$, corresponding to case (iii) in Fig. 3(a). This is signaled by the blue patches in Fig. 3(d), which we shall refer to as aligned patches.

The appearance of aligned patches is consistent with monolayer stress microscopy measurements on confluent

Madin-Darby canine kidney (MDCK) layers [42], which show that the area fraction of cells deformed in the direction of the active contractile filaments (along the first principal stress in the experiments) can be as large as 70%. Regions that are strongly correlated with straining flows, $\theta_{WQ} \approx 0$ or $\theta_{WQ} \approx \pi/2$, tend to lie between vortices where extensional/compressional flows dominate vorticity (see Fig. 6 in Appendix B).

As expected, θ_{WQ} shows a qualitatively different behavior with change in λ_Q in active turbulence driven by filaments with extensile activity, $\zeta > 0$. Here, the filaments are predominantly oriented along the extensional axis of the flow for all λ_Q as shown in Fig. 2(b). Hence $\theta_{WQ} \approx 0$ almost everywhere.

VII. TOPOLOGICAL DEFECTS FORMED BY ELONGATED CELLS AND ACTIVE FILAMENTS

Motile, long-lived $\pm\frac{1}{2}$ defects, which contribute to generating active flows, are characteristic of two-dimensional (2D) active turbulence [28,58,60]. However, in the study and analysis of defects in cellular layers [18,61–63] no distinction has yet been made between defects in the active filament and cell shape director fields. Our model allows us to make this distinction, and we find that defects are created in both the filament and the shape fields.

Figures 3(c) and 3(d) illustrate the position and orientation of filament and shape defects in a contractile system for $\lambda_Q = 0$ and $\lambda_Q = 0.8$ respectively. The defects tend to lie on the boundaries between aligned and misaligned patches, as observed in the measurements on epithelial monolayers [42]: this is natural as defects are locations with large changes in the orientation field. The figures show that the positions of the defects in shape and filaments are often correlated. However, even if the filament and shape defects are formed at the same location, they can take different relative orientations; the limiting cases for $+\frac{1}{2}$ defects are illustrated in Fig. 4(a). If the elongated cells and active filaments are aligned ($\theta_{WQ} \approx 0$), the $+\frac{1}{2}$ filament and shape defects point in the same direction. However, if the elongated cells and active filaments are orthogonal ($\theta_{WQ} \approx \pi/2$), the respective $+\frac{1}{2}$ defects take an antiparallel configuration, pointing in opposite directions. In our simulations, we more often find colocalized filament and shape defects in a parallel configuration in extensile systems and in an antiparallel configuration in contractile systems.

The asymmetry in the structure of a $+\frac{1}{2}$ topological defect formed by active filaments results in self-propulsion of the defect. The propulsion velocity is proportional to the activity of the filaments and is inversely proportional to the viscosity of the medium [64]. The direction of propulsion of the defect depends on the nature of activity: in an extensile system, the filament defects move towards their heads and in a contractile system the filament defects move towards their tails, as is well known from single-order parameter nematohydrodynamic theories [28]. On the other hand, $+\frac{1}{2}$ topological defects formed by the elongated cells do not self-propel, instead they are advected by the active turbulent flow field, often moving along with the associated filament $+\frac{1}{2}$ defect. Thus, as a consequence of the relative orientation of the filament and shape defects, in an aligned region the shape defects will also move towards their tails, whereas in a region with

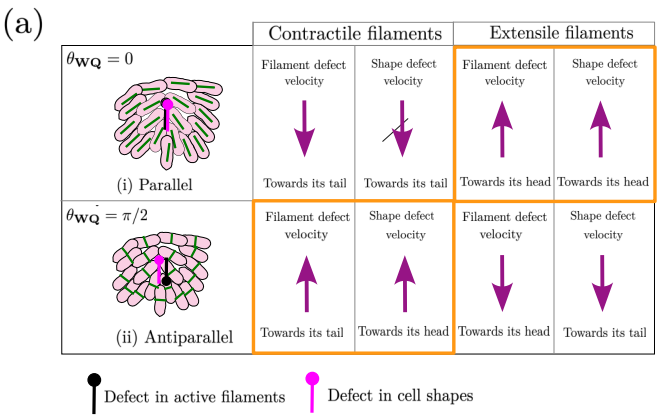

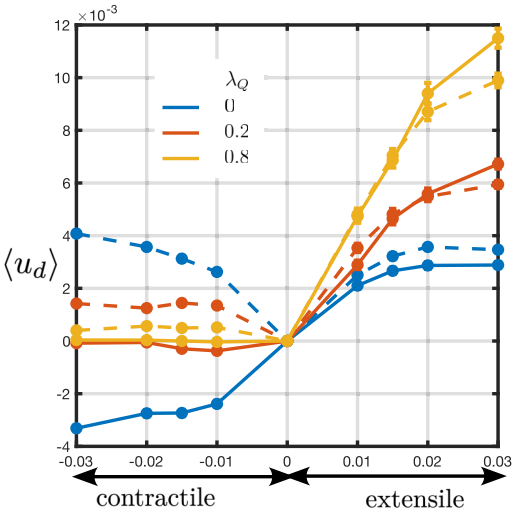

FIG. 4. Topological defects in the filament and shape fields. (a) Schematic illustrating the parallel (top) and antiparallel (bottom) configurations of colocalized $+\frac{1}{2}$ topological defects formed in regions where the cells and filaments are aligned ($\theta_{WQ} \approx 0$) or misaligned ($\theta_{WQ} \approx \frac{\pi}{2}$). Elongated cells are colored in pink, active filaments in green. The orientation of the shape and filament defects are indicated in magenta and black colors, respectively. Columns 2 and 3 indicate the velocity direction of the defects in contractile and extensile systems, respectively. Filament defects move towards their tails (heads) in contractile (extensile) systems; shape defects move with the filament defects. Boxes with orange outlines highlight scenarios predominantly observed in our simulations. (b) Average flow velocity $\langle u_d \rangle$ measured at the center of $+\frac{1}{2}$ shape and filament defects in extensile and contractile systems. $\langle u_d \rangle$ is defined as positive towards the head of the defect. he dashed (solid) lines 3 correspond to defects in cell shape (filaments).

$\theta_{WQ} \approx \pi/2$ they will move towards their heads. This is illustrated in Fig. 4(a) and provides an explanation for the heretofore puzzling observation that topological defects in confluent cell layers are observed to move towards their heads even though the cell filaments exert contractile forces.

The similarities and disparities arising in the dynamics of shape and filament defects can be illustrated from the simulation data by measuring the average fluid velocity at the center of $+\frac{1}{2}$ defects in an active turbulent flow field. This is plotted in Fig. 4(b). The velocity is defined positive in the direction of

orientation of the $+\frac{1}{2}$ defect, from tail to head. The magnitude of measured velocity increases with increasing activity for both shape and filament defects irrespective of whether the filaments are extensile or contractile. Moreover, as expected, the velocities at the center of shape and filament defects are comparable for extensile systems, and they increase with increasing filament flow-aligning parameter.

For contractile systems, since the change in filament flow-aligning parameter can change the distribution of θ_{EQ} [Fig. 2(c)], the difference in the apparent velocity measured at the center of filament and shape defects is also dependent on λ_Q. For $\lambda_Q = 0$, θ_{EQ} peaks at $\frac{\pi}{2}$. The shape and filament defects almost always move together in an antiparallel configuration, causing their velocities to be comparable in magnitude but oriented in opposite directions. This correlation reduces with an increase in the value of λ_Q [Fig. 2(a)] because of the decrease in the strength of active turbulent flow and because the shape and filament defects become less correlated in position and orientation [Figs. 2(c) and 3(d)].

VIII. SUMMARY

Using two tensor order parameters to differentiate the role of the force-generating active filament machinery in cells from the cells' shapes themselves, we construct a continuum theory to describe the dynamics of cellular layers and tissues. The theory shows that straining active flows generated by active filaments can elongate the otherwise isotropic cells, which form nematic domains the size of the active length scale. We discuss the properties of the active turbulent flow field, emphasising the relevance of a rheological quantity, the flow-aligning parameter of the filaments. As this increases, flow alignment of active filaments becomes more prevalent, and regions where the filament director field is parallel and regions where it is perpendicular to the straining flow can coexist in contractile active nematics. This agrees with the experimental observations of patches of alignment and misalignment between cell elongation and the direction of active stress in epithelial MDCK layers.

The mathematical framework introduced in our work to account for the deformation of cellular shape using a second tensor order parameter resembles the models used for modeling active viscoelastic fluids [65,66]. These works couple the two order parameters through a free energy, and the resulting elastic stress significantly alters the active flow field. However, in our simulations the two order parameters are coupled only through the underlying flow field, and the stress generated due to the shape deformations does not play a dominant role. This approach allows us to isolate the role of active flow fields in controlling the orientational and topological features of the cellular layers.

We distinguish topological defects generated in the filament director field, and in the cell elongation director field. In the former the defects move towards their tails (heads) in a contractile (extensile) system, as is well known from standard active nematic theories. Shape defects tend to be associated with filament defects, and move with them but point in a parallel (antiparallel) direction in aligned (misaligned) regions. Thus our approach explains why it is possible for the shape defects to move from tail to head even in a contractile system. The prediction of our model, which emerges from the misalignment of cell shape and filaments, can be tested experimentally by examining the orientation of filaments and cell shape around defects. Recent measurements in MDCK cell layers [43] show that stress fibers align with the cell shape in defects moving towards their tail, and misalign in defects moving towards their head. This supports our finding that active flows lead to cell elongation and that filaments are perpendicular to the cell shape around defects that move towards their head.

We note that considering intercellular nematic interactions, studied within the framework of multiphase-field models, has also predicted that defects can move in either direction [29,67]. Moreover, fluctuating polar forces in confluent cell layers lead to effective extensile nematic activity and hence shape defects that move towards their heads [68,69]. Therefore, further experimental and theoretical investigations are required to explain the observations of bidirectional motion of the defects [43] and to identify the extent to which each of these physical mechanisms contributes to the motion of topological defects in contractile cell monolayers. In addition, in this paper we consider a system of cells that have an isotropic shape in the absence of activity. This is more relevant for MDCK epithelial cells and undifferentiated HBECs, which typically exhibit a small and fluctuating anisotropic morphology. However, many other cell types, such as human mesothelial cell lines, C2C12 myoblasts, or NIH-3T3 fibroblasts, typically have elongated, spindle-like shapes. For these cells, the effect of filament and cell shape alignment becomes more important. As we showed in [42], strong alignment tends to shift the system toward a more contractile behavior, and in this regime we expect the $+1/2$ defects to preferentially move toward their tail. This is consistent with experimental observations, where defects primarily move toward their head in MDCK epithelial cells [18] and HBECs [36], but toward their tail in human mesothelial cell line LP-9 [42], C2C12 myoblasts, and NIH-3T3 fibroblasts [38]. A summary of these results is provided in Table I. It will be interesting to undertake a systematic study accounting for the active flow driven effects, as reported in this paper, together with anisotropic cell shapes in the future.

Our theory highlights the importance of distinguishing the roles of active filaments and cell shape, and reconciles the idea of contractile cells exhibiting extensile behavior, thus advancing the continuum modeling of cellular collectives. It also poses questions and suggests directions for new experiments on cell monolayers: we have referred to stress fibers and cytoskeletal force generating machinery as active filaments, but details of how these generate dipolar forces are unclear. In particular, it would be interesting to simultaneously measure filament and cell shape orientations to test the ideas presented here. Filament dynamics are difficult to follow, but may be accessible by perturbing monolayers by, e.g., stretching. We emphasise the importance of the filament and shape alignment parameters in determining the behavior of cell collectives. These are difficult parameters to measure as they will depend on details of the deformability of the cells and cell-cell interactions. Initial estimates could be obtained by measuring the response of a cell layer to a shear flow or by numerical experiments using multiphase field models. Moreover,

TABLE I. Cell morphology and direction of motion of $+1/2$ defects. Assuming that cells with large (small) anisotropy in their shape from experiments are equivalent to systems with more (less) shape and filament aligning effect in the simulations, the $+1/2$ defects predominantly move towards their tail (head) in both experiments and simulations [18,36,38,42].

Cell morphology	Large anisotropy	Small anisotropy
Cell name	C2C12 myoblasts and NIH-3T3 fibroblasts [38], human mesothelial cells [42]	MDCK epithelial cells [18], undifferentiated HBECs [36]
Filament and cell shape alignment in simulations	Important [42]	Less important (this work)
Dominant direction of motion of $+1/2$ defects (in experiments and simulations)	Towards tail	Towards head

measuring the velocity distribution of cells and of defects in the shape field, in experiments under varying conditions with different cell lines, will help to identify the physical regions of parameter space in the continuum model, and to identify any additional relevant physics.

In this study, we concentrate on nematic forces and ordering. There are many examples reported in the literature where polar forces [70,71] and different symmetries [35] are important in controlling the behavior of confluent cell layers. Our model can be extended to account for a polar field that captures the formation of polar structures and intracellular distributions by incorporating the dynamics of a polar order parameter. In addition, cell alignment can be influenced by the environment [72,73], and this would also be interesting to incorporate into our theory. A full picture of collective cell dynamics must work towards understanding the interplay between the different mechanisms for motility in varying cell lines, and in response to different genetic and chemical signals.

ACKNOWLEDGMENTS

We thank Jacob Notbohm for helpful discussions. J.M.Y. acknowledges support from the UK EPSRC (Award No. EP/W023849/1) and ERC Advanced Grant ActBio (funded as UKRI Frontier Research Grant No. EP/Y033981/1). This research was supported in part by Grant No. NSF PHY-2309135 to the Kavli Institute for Theoretical Physics (KITP). S.P.T. would like to thank the Royal Society and the Wolfson Foundation for a Royal Society Wolfson Fellowship award and acknowledges the support by the Department of Science and Technology, India, via the research Grant No. CRG/2023/000169.

DATA AVAILABILITY

The data are not publicly available. The data are available from the authors upon reasonable request.

APPENDIX A: TEMPORAL AUTOCORRELATION OF THE SHAPE TENSOR

The timescale of active flows, $\tau_a \sim \eta/\zeta$ can be obtained from the balance between the active stress and the viscous stress [Eq. (10) in the main text]. Since the flows result in the

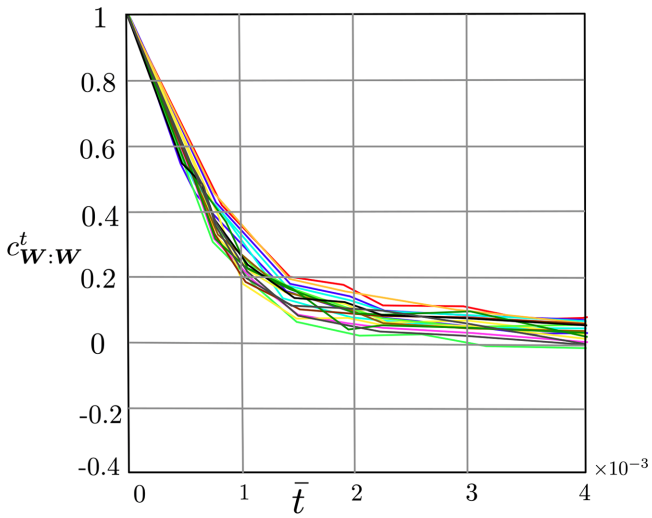

FIG. 5. Autocorrelation of the shape tensor $c^t_{W:W}$ as a function of rescaled time $\bar{t} = t\zeta/\eta$ for the same parameters as in Fig. 1(c).

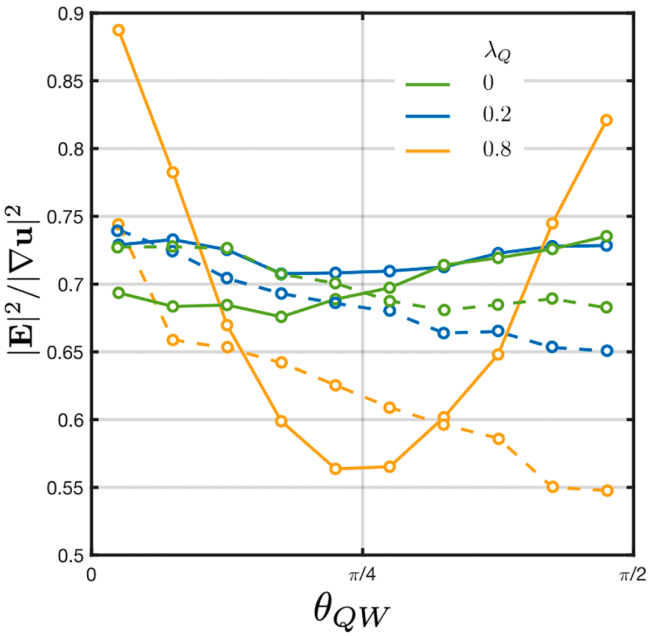

FIG. 6. The ratio of the straining flow to the total velocity gradient $|\boldsymbol{E}|^2/|\nabla \boldsymbol{u}|^2$ as a function of misalignment between filaments and cell shape $\theta_{\boldsymbol{QW}}$. The dashed (solid) lines show systems with extensile (contractile) filaments. The parameter values are the same as in Figs. 2(b) and 2(c).

deformation of cells, we calculated the autocorrelation of the shape tensor to determine the persistence time of the deformed cells. The autocorrelation function is calculated as $c^t_{\boldsymbol{W}:\boldsymbol{W}} = \langle \boldsymbol{W}(r, t_0 + t) : \boldsymbol{W}(r, t_0)\rangle_{r,t_0} / \langle \boldsymbol{W}(r, t_0) : \boldsymbol{W}(r, t_0)\rangle_{r,t_0}$, where the average $\langle\rangle_{r,t_0}$ is defined over space r and time t_0, and plotted in Fig. 5 for the same range of parameters as in Fig. 1(c) in the main text. As is evident from the figure, the decorrelation time of the shape tensor is approximately correlated with the active timescale τ_a.

APPENDIX B: STRONGER EXTENSIONAL FLOWS IN ALIGNED AND MISALIGNED REGIONS

In order to show the effect of straining flows in determining the regions of alignment and misalignment between the active filaments and elongated cells, we plot in Fig. 6 the ratio of the straining flow to the total velocity gradient $|\boldsymbol{E}|^2/|\nabla \boldsymbol{u}|^2$ as a function of misalignment angle between filaments and cell shape $\theta_{\boldsymbol{QW}}$. The dashed (solid) line shows a system with extensile (contractile) filaments. It may be seen that the distribution is monotonic in extensile systems irrespective of the value of $\lambda_{\boldsymbol{Q}}$. However, for large λ_Q in contractile systems, the regions of alignment ($\theta_{\boldsymbol{QW}} \approx 0$) and misalignment ($\theta_{\boldsymbol{QW}} \approx \frac{\pi}{2}$) correspond to regions with relatively larger contribution of rate of strain tensor to the velocity gradient.

Movies

See the Supplemental Material [74] for the following additional visual aids.

Movie 1. Dynamics of a system with contractile active filaments, with filament flow aligning parameter $\lambda_Q = 0$. Left panel: cell shape orientation and defects in the cell shape field. The background color shows the magnitude of the cell elongation $|\boldsymbol{W}|$. Right panel: active flows are shown as streamlines; defects in cell shape (filaments) are shown in magenta (black). The background color shows the misalignment angle $\theta_{\boldsymbol{QW}}$. For a zero filament shear alignment, the cell shape is almost everywhere perpendicular to the the filament orientation.

Movie 2. Dynamics of a system with contractile active filaments, with filament flow aligning parameter $\lambda_Q = 0.8$. Left panel: cell shape orientation and defects in the cell shape field. The background color shows the magnitude of the cell elongation $|\boldsymbol{W}|$. Right panel: active flows are shown as streamlines; defects in cell shape (filaments) are shown in magenta (black). The background color shows the misalignment angle $\theta_{\boldsymbol{QW}}$. For a nonzero filament shear alignment, the monolayer forms regions where cell shape is aligned with the filament orientation.

[1] G. Gompper, R. G. Winkler, T. Speck, A. Solon, C. Nardini, F. Peruani, H. Löwen, R. Golestanian, U. B. Kaupp, L. Alvarez *et al.*, The 2020 motile active matter roadmap, J. Phys.: Condens. Matter **32**, 193001 (2020).

[2] O. Hallatschek, S. S. Datta, K. Drescher, J. Dunkel, J. Elgeti, B. Waclaw, and N. S. Wingreen, Proliferating active matter, Nat. Rev. Phys. **5**, 407 (2023).

[3] M. J. Bowick, N. Fakhri, M. C. Marchetti, and S. Ramaswamy, Symmetry, thermodynamics, and topology in active matter, Phys. Rev. X **12**, 010501 (2022).

[4] J. M. Yeomans, Mechanobiology, in *Oxford Research Encyclopedia of Physics* (Oxford University Press, Oxford, 2023).

[5] J.-F. Joanny and L. Brézin, Tissues as active materials, in *Active Matter and Nonequilibrium Statistical Physics: Lecture Notes of the Les Houches Summer School* (Oxford University Press, Oxford, 2022), Vol. 112, p. 307.

[6] E. W. Gehrels, B. Chakrabortty, M.-E. Perrin, M. Merkel, and T. Lecuit, Curvature gradient drives polarized tissue flow in the *Drosophila* embryo, Proc. Natl. Acad. Sci. USA **120**, e2214205120 (2023).

[7] R. M. Herrera-Perez, C. Cupo, C. Allan, A. B. Dagle, and K. E. Kasza, Tissue flows are tuned by actomyosin-dependent mechanics in developing embryos, PRX Life **1**, 013004 (2023).

[8] R. J. Tetley, M. F. Staddon, D. Heller, A. Hoppe, S. Banerjee, and Y. Mao, Tissue fluidity promotes epithelial wound healing, Nat. Phys. **15**, 1195 (2019).

[9] R. Alert and X. Trepat, Physical models of collective cell migration, Annu. Rev. Condens. Matter Phys. **11**, 77 (2020).

[10] E. Lång, A. Lång, P. Blicher, T. Rognes, P. G. Dommersnes, and S. O. Bøe, Topology-guided polar ordering of collective cell migration, Sci. Adv. **10**, eadk4825 (2024).

[11] S. Grosser, J. Lippoldt, L. Oswald, M. Merkel, D. M. Sussman, F. Renner, P. Gottheil, E. W. Morawetz, T. Fuhs, X. Xie, S. Pawlizak, A. W. Fritsch, B. Wolf, L.-C. Horn, S. Briest, B. Aktas, M. L. Manning, and J. A. Käs, Cell and nucleus shape as an indicator of tissue fluidity in carcinoma, Phys. Rev. X **11**, 011033 (2021).

[12] S. B. Lemke and C. M. Nelson, Dynamic changes in epithelial cell packing during tissue morphogenesis, Curr. Biol. **31**, R1098 (2021).

[13] C. Villeneuve, A. Hashmi, I. Ylivinkka, E. Lawson-Keister, Y. A. Miroshnikova, C. Pérez-González, S.-M. Myllymäki, F. Bertillot, B. Yadav, T. Zhang *et al.*, Mechanical forces across compartments coordinate cell shape and fate transitions to generate tissue architecture, Nat. Cell Biol. **26**, 207 (2024).

[14] F. Ascione, S. Caserta, S. Esposito, V. R. Villella, L. Maiuri, M. R. Nejad, A. Doostmohammadi, J. M. Yeomans, and S. Guido, Collective rotational motion of freely-expanding T84 epithelial cell colonies, J. R. Soc. Interface. **20**, 20220719 (2023).

[15] M. Saadaoui, D. Rocancourt, J. Roussel, F. Corson, and J. Gros, A tensile ring drives tissue flows to shape the gastrulating amniote embryo, Science **367**, 453 (2020).

[16] G. Duclos, C. Blanch-Mercader, V. Yashunsky, G. Salbreux, J.-F. Joanny, J. Prost, and P. Silberzan, Spontaneous shear flow in confined cellular nematics, Nat. Phys. **14**, 728 (2018).

[17] A. Saraswathibhatla, S. Henkes, E. E. Galles, R. Sknepnek, and J. Notbohm, Coordinated tractions increase the size of a

collectively moving pack in a cell monolayer, Extreme Mech. Lett. **48**, 101438 (2021).
[18] T. B. Saw, A. Doostmohammadi, V. Nier, L. Kocgozlu, S. Thampi, Y. Toyama, P. Marcq, C. T. Lim, J. M. Yeomans, and B. Ladoux, Topological defects in epithelia govern cell death and extrusion, Nature (London) **544**, 212 (2017).
[19] R. Alert, J.-F. Joanny, and J. Casademunt, Universal scaling of active nematic turbulence, Nat. Phys. **16**, 682 (2020).
[20] B. H. Lee, I. Seijo-Barandiaran, and A. Grapin-Botton, Epithelial morphogenesis in organoids, Curr. Opin. Genetics Dev. **72**, 30 (2022).
[21] J. Devany, D. M. Sussman, T. Yamamoto, M. L. Manning, and M. L. Gardel, Cell cycle–dependent active stress drives epithelia remodeling, Proc. Natl. Acad. Sci. USA **118**, e1917853118 (2021).
[22] K. E. Cavanaugh, M. F. Staddon, E. Munro, S. Banerjee, and M. L. Gardel, RhoA mediates epithelial cell shape changes via mechanosensitive endocytosis, Dev. Cell **52**, 152 (2020).
[23] J. Dunkel, S. Heidenreich, K. Drescher, H. H. Wensink, M. Bär, and R. E. Goldstein, Fluid dynamics of bacterial turbulence, Phys. Rev. Lett. **110**, 228102 (2013).
[24] H. H. Wensink, J. Dunkel, S. Heidenreich, K. Drescher, R. E. Goldstein, H. Löwen, and J. M. Yeomans, Meso-scale turbulence in living fluids, Proc. Natl. Acad. Sci. USA **109**, 14308 (2012).
[25] A. Opathalage, M. M. Norton, M. P. Juniper, B. Langeslay, S. A. Aghvami, S. Fraden, and Z. Dogic, Self-organized dynamics and the transition to turbulence of confined active nematics, Proc. Natl. Acad. Sci. USA **116**, 4788 (2019).
[26] J. Prost, F. Jülicher, and J.-F. Joanny, Active gel physics, Nat. Phys. **11**, 111 (2015).
[27] T. B. Saw, W. Xi, B. Ladoux, and C. T. Lim, Biological tissues as active nematic liquid crystals, Adv. Mater. **30**, 1802579 (2018).
[28] A. Doostmohammadi, J. Ignés-Mullol, J. M. Yeomans, and F. Sagués, Active nematics, Nat. Commun. **9**, 3246 (2018).
[29] L. Balasubramaniam, A. Doostmohammadi, T. B. Saw, G. H. N. S. Narayana, R. Mueller, T. Dang, M. Thomas, S. Gupta, S. Sonam, A. S. Yap, Y. Toyama, R.-M. Mège, J. M. Yeomans, and B. Ladoux, Investigating the nature of active forces in tissues reveals how contractile cells can form extensile monolayers, Nat. Mater. **20**, 1156 (2021).
[30] J.-F. Joanny and J. O. Indekeu, Statistical physics of active matter, cell division and cell aggregation, Physica A **631**, 129314 (2023).
[31] A. Doostmohammadi, S. P. Thampi, and J. M. Yeomans, Defect-mediated morphologies in growing cell colonies, Phys. Rev. Lett. **117**, 048102 (2016).
[32] S. Shankar, A. Souslov, M. J. Bowick, M. C. Marchetti, and V. Vitelli, Topological active matter, Nat. Rev. Phys. **4**, 380 (2022).
[33] H. Xu, M. R. Nejad, J. M. Yeomans, and Y. Wu, Geometrical control of interface patterning underlies active matter invasion, Proc. Natl. Acad. Sci. USA **120**, e2219708120 (2023).
[34] F. Vafa and L. Mahadevan, Active nematic defects and epithelial morphogenesis, Phys. Rev. Lett. **129**, 098102 (2022).
[35] J.-M. Armengol-Collado, L. N. Carenza, J. Eckert, D. Krommydas, and L. Giomi, Epithelia are multiscale active liquid crystals, Nat. Phys. **19**, 1773 (2023).
[36] C. Blanch-Mercader, V. Yashunsky, S. Garcia, G. Duclos, L. Giomi, and P. Silberzan, Turbulent dynamics of epithelial cell cultures, Phys. Rev. Lett. **120**, 208101 (2018).
[37] M. R. Nejad and J. M. Yeomans, Spontaneous rotation of active droplets in two and three dimensions, PRX Life **1**, 023008 (2023).
[38] G. Duclos, C. Erlenkämper, J.-F. Joanny, and P. Silberzan, Topological defects in confined populations of spindle-shaped cells, Nat. Phys. **13**, 58 (2017).
[39] M. Czajkowski, D. Bi, M. L. Manning, and M. C. Marchetti, Hydrodynamics of shape-driven rigidity transitions in motile tissues, Soft Matter **14**, 5628 (2018).
[40] A. Hernandez and M. C. Marchetti, Poisson-bracket formulation of the dynamics of fluids of deformable particles, Phys. Rev. E **103**, 032612 (2021).
[41] M. Doi and T. Ohta, Dynamics and rheology of complex interfaces. I, J. Chem. Phys. **95**, 1242 (1991).
[42] M. R. Nejad, L. J. Ruske, M. McCord, J. Zhang, G. Zhang, J. Notbohm, and J. M. Yeomans, Stress-shape misalignment in confluent cell layers, Nat. Commun. **15**, 3628 (2024).
[43] P. K. Bera, M. McCord, J. Zhang, J. Notbohm, Traction and stress control formation and motion of +1/2 topological defects in epithelial cell monolayers, Newton **1**, 100231 (2025).
[44] P. G. de Gennes and J. Prost, *The Physics of Liquid Crystals* (Oxford University Press, Oxford, 1995).
[45] A. N. Beris and B. J. Edwards, *Thermodynamics of Flowing Systems: With Internal Microstructure* (Oxford University Press, Oxford, 1994).
[46] R. A. Simha and S. Ramaswamy, Hydrodynamic fluctuations and instabilities in ordered suspensions of self-propelled particles, Phys. Rev. Lett. **89**, 058101 (2002).
[47] T. Sanchez, D. T. Chen, S. J. DeCamp, M. Heymann, and Z. Dogic, Spontaneous motion in hierarchically assembled active matter, Nature (London) **491**, 431 (2012).
[48] J. Colen, M. Han, R. Zhang, S. A. Redford, L. M. Lemma, L. Morgan, P. V. Ruijgrok, R. Adkins, Z. Bryant, Z. Dogic *et al.*, Machine learning active-nematic hydrodynamics, Proc. Natl. Acad. Sci. USA **118**, e2016708118 (2021).
[49] Y. Hatwalne, S. Ramaswamy, M. Rao, and R. A. Simha, Rheology of active-particle suspensions, Phys. Rev. Lett. **92**, 118101 (2004).
[50] M. Luciano, M. Versaevel, E. Vercruysse, A. Procès, Y. Kalukula, A. Remson, A. Deridoux, and S. Gabriele, Appreciating the role of cell shape changes in the mechanobiology of epithelial tissues, Biophys. Rev. **3**, 011305 (2022).
[51] K. Schakenraad, J. Ernst, W. Pomp, E. H. J. Danen, R. M. H. Merks, T. Schmidt, and L. Giomi, Mechanical interplay between cell shape and actin cytoskeleton organization, Soft Matter **16**, 6328 (2020).
[52] M. Nejad and J. M. Yeomans, Coarse-graining dense, deformable active particles, arXiv:2501.07280.
[53] D. Marenduzzo, E. Orlandini, M. E. Cates, and J. M. Yeomans, Steady-state hydrodynamic instabilities of active liquid crystals: Hybrid lattice Boltzmann simulations, Phys. Rev. E **76**, 031921 (2007).
[54] S. P. Thampi, R. Golestanian, and J. M. Yeomans, Vorticity, defects and correlations in active turbulence, Philos. Trans. R. Soc. A **372**, 20130366 (2014).
[55] L. C. Head, C. Doré, R. R. Keogh, L. Bonn, G. Negro, D. Marenduzzo, A. Doostmohammadi, K. Thijssen, T. López-

León, and T. N. Shendruk, Spontaneous self-constraint in active nematic flows, Nat. Phys. **20**, 492 (2024).

[56] S. P. Thampi, R. Golestanian, and J. M. Yeomans, Instabilities and topological defects in active nematics, Europhys. Lett. **105**, 18001 (2014).

[57] L. Giomi, M. J. Bowick, X. Ma, and M. C. Marchetti, Defect annihilation and proliferation in active nematics, Phys. Rev. Lett. **110**, 228101 (2013).

[58] L. Giomi, M. J. Bowick, P. Mishra, R. Sknepnek, and M. C. Marchetti, Defect dynamics in active nematics, Philos. Trans. R. Soc. A **372**, 20130365 (2014).

[59] I. Vélez-Cerón, P. Guillamat, F. Sagués, and J. Ignés-Mullol, Probing active nematics with in situ microfabricated elastic inclusions, Proc. Natl. Acad. Sci. USA **121**, e2312494121 (2024).

[60] M. Serra, L. Lemma, L. Giomi, Z. Dogic, and L. Mahadevan, Defect-mediated dynamics of coherent structures in active nematics, Nat. Phys. **19**, 1355 (2023).

[61] D. Zhang, P. Chen, Z. Li, R. Zhang, and B. Li, Topological defect-mediated morphodynamics of active–active interfaces, Proc. Natl. Acad. Sci. USA **119**, e2122494119 (2022).

[62] A. Ardaševa and A. Doostmohammadi, Topological defects in biological matter, Nat. Rev. Phys. **4**, 354 (2022).

[63] K. Kawaguchi, R. Kageyama, and M. Sano, Topological defects control collective dynamics in neural progenitor cell cultures, Nature (London) **545**, 327 (2017).

[64] J. Rønning, M. C. Marchetti, M. J. Bowick, and L. Angheluta, Flow around topological defects in active nematic films, Proc. R. Soc. A **478**, 20210879 (2022).

[65] E. J. Hemingway, A. Maitra, S. Banerjee, M. C. Marchetti, S. Ramaswamy, S. M. Fielding, and M. E. Cates, Active viscoelastic matter: From bacterial drag reduction to turbulent solids, Phys. Rev. Lett. **114**, 098302 (2015).

[66] E. J. Hemingway, M. Cates, and S. M. Fielding, Viscoelastic and elastomeric active matter: Linear instability and nonlinear dynamics, Phys. Rev. E **93**, 032702 (2016).

[67] G. Zhang and J. M. Yeomans, Active forces in confluent cell monolayers, Phys. Rev. Lett. **130**, 038202 (2023).

[68] A. Killeen, T. Bertrand, and C. F. Lee, Polar fluctuations lead to extensile nematic behavior in confluent tissues, Phys. Rev. Lett. **128**, 078001 (2022).

[69] L. Bonn, A. Ardaševa, R. Mueller, T. N. Shendruk, and A. Doostmohammadi, Fluctuation-induced dynamics of nematic topological defects, Phys. Rev. E **106**, 044706 (2022).

[70] B. Aigouy, R. Farhadifar, D. B. Staple, A. Sagner, J.-C. Röper, F. Jülicher, and S. Eaton, Cell flow reorients the axis of planar polarity in the wing epithelium of *Drosophila*, Cell **142**, 773 (2010).

[71] S. Jain, V. M. L. Cachoux, G. H. N. S. Narayana, S. de Beco, J. D'Alessandro, V. Cellerin, T. Chen, M. L. Heuze, P. Marcq, R.-M. Mege, A. J. Kabla, C. T. Lim, and B. Ladoux, The role of single-cell mechanical behaviour and polarity in driving collective cell migration, Nat. Phys. **16**, 802 (2020).

[72] R. M. Adar and J.-F. Joanny, Environment-stored memory in active nematics and extra-cellular matrix remodeling, Phys. Rev. Lett. **133**, 118402 (2024).

[73] S. Bell, J. Ackermann, A. Maitra, and R. Voituriez, Ordering spontaneous flows and aging in active fluids depositing tracks, Phys. Rev. E **111**, L023405 (2025).

[74] See Supplemental Material at http://link.aps.org/supplemental/10.1103/mmyk-f9x3 for details of the methods used to analyze the data.